Cell-Free Massive MIMO With Mixed-Resolution ADCs and I/Q Imbalance Over Rician Spatially Correlated Channels

Zhilong Liu , *Graduate Student Member, IEEE*,
Jiayi Zhang , *Senior Member, IEEE*, Zhe Wang ,
Xiaodan Zhang , Huahua Xiao, and Bo Ai , *Fellow, IEEE*

Abstract—The practical deployment of cell-free massive multiple-input multiple-output (CF mMIMO), a promising technology empowering the sixth-generation with multitudinous access points (APs). This paper considers a CF mMIMO system over Rician spatially correlated fading channels with the single-antenna user equipments (UEs) and multi-antenna APs, where the phase-shift induced by the UEs' movement exists at the line-of-sight path. Though the low-resolution analog-to-digital converters (ADCs) can effectively address the expensive hardware cost and power-hungry problems, complicated data processing algorithms are of vital importance to be well designed to compensate for the performance gap compared with the real scenarios since the hardware impairments. However, the novel mixed-ADC architecture could solve the above challenges with better performance. So, we investigate the effect of mixed-resolution ADCs deploying at APs and the in-phase and quadrature-phase imbalance (IQI) on the CF mMIMO systems. Furthermore, the achievable uplink spectral efficiency (SE) is analyzed considering IQI and quantization loss based on a two-layer decoding scheme. Moreover, the novel closed-form SE expression with the maximum ratio (MR) combining is derived. And we find the relationship between the SE performance and different combining schemes, quantization bits, and IQI parameters. Finally, the numerical results reveal the mixed-resolution ADCs show a great advantage in boosting the SE performance, and increasing the number of APs is an effective means to promote the system performance.

Index Terms—Cell-free massive MIMO, I/Q imbalance, mixed-resolution ADC, spectral efficiency.

I. INTRODUCTION

Over the past few decades, the academy has proposed advanced technologies to meet the unprecedented growth of wireless data throughput, such as multiple-input multiple-output (MIMO) [1], reconfigurable

Zhilong Liu, Jiayi Zhang, and Zhe Wang are with the School of Electronic and Information Engineering, Beijing Jiaotong University, Beijing 100044, China, and also with the Frontiers Science Center for Smart High-speed Railway System, Beijing 100044, China (e-mail: 22110038@bjtu.edu.cn; jiayizhang@bjtu.edu.cn; 20111050@bjtu.edu.cn).

Xiaodan Zhang is with the School of Management, Shenzhen Institute of Information Technology, Shenzhen 518172, China (e-mail: zhangxd@sziit.edu.cn).

Huahua Xiao is with the ZTE Corporation, State Key Laboratory of Mobile Network and Mobile Multimedia Technology, Shenzhen 518055, China (e-mail: xiao.huahua@zte.com.cn).

Bo Ai is with the State Key Laboratory of Rail Traffic Control and Safety, Beijing Jiaotong University, Beijing 100044, China (e-mail: boai@bjtu.edu.cn).

Digital Object Identifier 10.1109/TVT.2023.3244940

intelligent surface (RIS) [2], [3], TeraHertz (THz) communication technology [4] and so on. The traditional communication paradigms are undergoing a landmark revolution to access the next-generation communication system.

MIMO, a vital physical layer technology of the fifth-generation (5G), provides both diversity and spatial reuse to enhance the transmission reliability and the transmission rate [5]. However, limited by the system architecture and the sharp increase in the network throughput, the industry puts forward new demands to the forthcoming wireless communication. Cell-free massive MIMO (CF mMIMO), promoting the spectral efficiency (SE) by introducing the thought of "user-centric," can address the inter-cell interference existing at the implementation of "cell-centric" networks and cope with the challenges brought by the exponential growth of mobile data traffic due to its outstanding advantages of fully exploiting the spatial degrees-of-freedom [6], [7], [8]. In CF mMIMO systems, a good deal of access points (APs) with massive antenna arrays are distributed at the service region and coordinate with each other to serve all user equipments (UEs) [9]. It is noteworthy that the key performance indicators for evaluating the CF mMIMO are SE and energy efficiency (EE). For instance, a low-complexity power control algorithm based on the accelerated projected gradient method was proposed for EE maximization in [10], while the uplink SE performance of CF mMIMO system with multi-antenna UEs over spatially correlated Rayleigh fading channels was effectively analyzed in [7]. Nevertheless, the hardware cost and power consumption of APs are still pendent challenges in the sixth-generation.

In CF mMIMO, the number of radio-frequency links implemented at APs is proportional to the number of antennas, which undoubtedly brings considerable data processing burden, expensive hardware cost, and high system power consumption. In order to tackle the aforementioned issues, a novel method, adopting low-precision components was proposed. The uplink performance with the low-resolution analog-to-digital converters (ADCs) over Weichselberger Rayleigh fading channels was investigated in [11]. However, the assumption of APs with all antennas connected to high-resolution ADCs will be quite power-hungry, while the low-resolution ADCs are at the cost of SE degradation. In contrast, the mixed-ADC architecture can achieve a balance between EE and SE [12], remarkably reducing the hardware cost and power consumption. In [13], the alternating optimization method was attempted to jointly solve the power control problem and antenna selection with the APs equipped with the mixed-ADC architecture. Aside from [13], the max-min fairness algorithm was valid for optimizing power in CF mMIMO systems [12].

Typically, the digital communication systems are undergoing the effect of hardware impairments, introduced by low-resolution components, such as phase noise, in-phase or quadrature-phase imbalance (IQI), and others [14]. The EE performance of CF mMIMO systems over the Rayleigh channels was investigated under the limited fronthaul capacity and low-resolution ADCs in [15]. And the hardware-quality scaling law shed light on the potential relationship between hardware impairments and the number of antennas [16]. Recently, the uplink achievable rate expressions were derived over the Rayleigh fading channels with compress-forward strategies [17] and the eavesdroppers [18], respectively. Unfortunately, the state-of-the-art researches are mainly focused on the Rayleigh fading channels [14], [15], [16], [17], [18]. While with the combination of line-of-sight (LoS) path and small-scale fading in the real CF mMIMO systems [19], the Rician fading channels

are more suitable for the actual wireless propagation channel modeling in CF mMIMO systems [20].

Motivated by the aforementioned observations, in this paper, we consider a CF mMIMO system with the mixed-resolution ADCs architecture and IQI at multi-antenna APs over Rician spatially correlated fading channels with phase-shifts. The main contributions are given as follows:

- Based on the phase-aware minimum mean squared error (MMSE) channel estimator, we derive the SE expressions for different combining schemes. More specifically, we derive exact closed-form uplink SE expressions for MR combining with mixed-ADC architecture and IQI.
- We reveal the impacts of different combining schemes, the number of quantization bits, and IQI parameters on the uplink SE performance. Compared with MR combining, the SE performance of the mixed-ADC architecture with L-MMSE combining is more advantageous. Our analysis unveils that hardware impairments have significant impacts on the performance of CF mMIMO systems.

The rest of this paper is organized as follows. The CF mMIMO system model with IQI and mixed-resolution ADCs is briefly introduced in Section II. Then, the uplink SE performance and closed-form SE expressions with MR combining based on the large-scale fading decoding (LSFD) scheme of such a system are derived in Section III. Finally, Section IV provides the simulation results and discussion to illustrate the effects of mixed-ADC architecture and IQI, while the conclusions are drawn in Section V.

II. SYSTEM MODEL

An uplink CF mMIMO network is investigated which consists of M APs equipped with L antennas each and K single-antenna UEs. All APs connect to a central processing unit (CPU) via lossless fronthaul links [3], [7], [9]. The system operates in the time division duplexing (TDD) mode where the channel responses remain constant over a coherence block of τ_c samples. Note that τ_p samples are reserved for training and the remaining $\tau_u = \tau_c - \tau_p$ are reserved for payload data. The channel response between L antennas of AP m and UE k is denoted by $\mathbf{h}_{mk} \in \mathbb{C}^L$, which is assumed to keep constant over a coherence time block of τ_c channel uses.

A. Rician Correlated Fading Channels With Phase-Shifts

In this paper, we consider the Rician spatially correlated fading channel which is comprised of a semi-deterministic LoS path component with a random phase-shift and a stochastic non-line-of-sight (NLoS) path component [19] as $\mathbf{h}_{mk} = \bar{\mathbf{h}}_{mk}\mathbf{P}_{mk} + \mathbf{g}_{mk}$, where $\bar{\mathbf{h}}_{mk}$ is the deterministic LoS path component, $\mathbf{g}_{mk} \sim \mathcal{N}_{\mathbb{C}}(\mathbf{0}, \mathbf{R}_{mk})$ is the NLoS component, and $\mathbf{R}_{mk} \in \mathbb{C}^{L \times L}$ is the positive semi-definite covariance matrix describing the spatial correlation of $\mathbf{g}_{mk}$, respectively. In addition, the phase-shift matrix $\mathbf{P}_{mk} = \mathrm{diag}(e^{j\varphi_{mk,1}}, \ldots, e^{j\varphi_{mk,L}}) \in \mathbb{C}^{L \times L}$ describes the phase-shift of AP m and UE k, where the l-th element $\varphi_{mk,l} \sim \mathcal{U}(-\pi, \pi)$ represents the phase-shift of the LoS component between the l-th antenna of AP m and UE k [19]. We assume that the diagonal elements of $\mathbf{P}_{mk}$ are equal to φ_{mk}, so $\mathbf{h}_{mk}$ can be rewritten as

$$\mathbf{h}_{mk} = \bar{\mathbf{h}}_{mk}e^{j\varphi_{mk}} + \mathbf{g}_{mk}, \tag{1}$$

where φ_{mk} and the channel realization $\mathbf{h}_{mk}$ are assumed independent and identically distributed (i.i.d.) random variables in different coherence blocks.

TABLE I
DISTORTION FACTORS FOR DIFFERENT QUANTIZATION BITS

b_l	1	2	3	4	5
ρ_l	0.6366	0.8825	0.96546	0.990503	0.997501

On the other hand, the large-scale fading coefficient between AP m and UE k, $\beta_{mk}^{\mathrm{NLoS}} = \frac{\mathrm{tr}(\mathbf{R}_{mk})}{LN}$, describes the geometric pathloss and shadowing for the NLoS path.

B. Channel Estimation

In this phase, the channel state information (CSI) is gathered at the APs. Each AP can only exploit its local CSI for receive signals combining [9]. We assume that τ_p mutually orthogonal τ_p-length pilot sequences are used for channel estimation. $\phi_k \in \mathbb{C}^{\tau_p}$ denotes the pilot sequence of UE k, with $\|\phi_k\|^2 = \tau_p$. We define $\mathcal{P}_k$ as the set of UEs that use the same pilot sequence as UE k, including itself. With $\hat{p}_k$ being the pilot transmit power of UE k, the pilot sequences are sent by all the UEs to the APs. Then the received pilot signal $\mathbf{y}_m^p \in \mathbb{C}^{L \times \tau_p}$ at AP m is $\mathbf{y}_m^p = \sum_{k=1}^{K} \sqrt{\hat{p}_k}\mathbf{h}_{mk}\phi_k^T + \mathbf{n}_m^p$, where $\mathbf{n}_m^p \sim \mathcal{N}_{\mathbb{C}}(\mathbf{0}, \sigma^2\mathbf{I}_L)$ is the additive noise with σ^2 denoting the noise power. Affected by IQI, we consider it at the AP side based on the asymmetrical IQI model [11], so that the received pilot signal $\mathbf{y}_{iqi,m}^p$ at AP m can be expressed as

$$\mathbf{y}_{iqi,m}^p = \mathbf{K}_{1,m}\mathbf{y}_m^p + \mathbf{K}_{2,m}\left(\mathbf{y}_m^p\right)^*$$

$$= \sum_{k=1}^{K} \sqrt{\hat{p}_k}\mathbf{K}_{1,m}\mathbf{h}_{mk}\phi_k^T + \sum_{k=1}^{K} \sqrt{\hat{p}_k}\mathbf{K}_{2,m}\mathbf{h}_{mk}^*\phi_k^H$$

$$+ \mathbf{n}_{iqi,m}^p, \tag{2}$$

where $\mathbf{n}_{iqi,m}^p = \mathbf{K}_{1,m}\mathbf{n}_m^p + \mathbf{K}_{2,m}(\mathbf{n}_m^p)^* \sim \mathcal{N}_{\mathbb{C}}(\mathbf{0}, \mathbf{\Xi})$ and $\mathbf{\Xi} = (|\mathbf{K}_{1,m}|^2 + |\mathbf{K}_{2,m}|^2)\sigma^2$. The diagonal matrix $\mathbf{K}_{1,m} = \mathrm{diag}(\mathbf{K}_{1,m}^1, \ldots, \mathbf{K}_{1,m}^L) \in \mathbb{C}^{L \times L}$ and $\mathbf{K}_{2,m} = \mathrm{diag}(\mathbf{K}_{2,m}^1, \ldots, \mathbf{K}_{2,m}^L) \in \mathbb{C}^{L \times L}$ denote the IQI coefficient matrix of AP m with the diagonal entries $\mathbf{K}_{1,m}^l = \frac{1}{2}(1 + g_l e^{-j\theta_l})$ and $\mathbf{K}_{2,m}^l = \frac{1}{2}(1 - g_l e^{j\theta_l})$, where g_l and θ_l denote the amplitude and phase mismatch, respectively.

Compared with the traditional perfect ADCs causing a huge power consumption and low-resolution ADCs strategy decreasing the SE, we consider a mixed-ADC architecture in this paper, which achieves the tradeoff between the SE performance and hardware cost. Since the ADCs with different resolutions are disposed at the antennas of APs, so the quantization bits of each antenna can be expressed as $\mathbf{b} = [b_1, \ldots, b_L]$, where b_l can be the arbitrary integer from one bit to the maximum value of the ADCs.

The received signal at AP m being quantized can be indicated on the basis of the linear additive quantization noise model (AQNM) [12] as $\check{\mathbf{y}}_m^p = \mathcal{Q}(\mathbf{y}_{iqi,m}^p) = \mathbf{A}\mathbf{y}_{iqi,m}^p + \check{\mathbf{n}}_{mq}^p$, where $\mathbf{A} = \mathrm{diag}(\alpha_1, \ldots, \alpha_L)$ and $\check{\mathbf{n}}_{mq}^p$ is the additive Gaussian quantization noise which is uncorrelated with $\mathbf{y}_{iqi,m}^p$, respectively. And $\alpha_l = 1 - \rho_l$ is the linear gain, where ρ_l is the inverse of the signal-to-quantization-noise ratio, depending on the quantization bits of ADCs. Accordingly, the relationship between ρ_l and b_l is shown in Table I for $b_l \leq 5$, and can be modeled as $\rho_l = \frac{\pi\sqrt{3}}{2} \cdot 2^{-2b_m}$ when $b_l > 6$ [13]. And the covariance matrix of the quantization noise $\check{\mathbf{n}}_{mq}^p$ is given by (3) shown at the bottom of the next page.

In order to acquire sufficient statistics to estimate the channel, we first multiple the quantization signal $\check{\mathbf{y}}_m^p$ with ϕ_k^* to obtain $\mathbf{y}_{mk}^p = \check{\mathbf{y}}_m^p \phi_k^*$ as $\mathbf{y}_{mk}^p = \sum_{k=1}^K \sqrt{\hat{p}_k} \mathbf{A}\mathbf{K}_{1,m}\mathbf{h}_{mk}\phi_k^T\phi_k^* + \sum_{k=1}^K \sqrt{\hat{p}_k}\mathbf{A}\mathbf{K}_{2,m}\mathbf{h}_{mk}^*\phi_k^H\phi_k^* + \mathbf{A}\mathbf{n}_{iqi,m}^p\phi_k^* + \check{\mathbf{n}}_{mq}^p\phi_k^*$. Since there are a great number of UEs deployed in the CF mMIMO systems such that $\tau_p < K$, and the pilots are mutually orthogonal, so $\mathbf{y}_{mk}^p$ can be rewritten as $\mathbf{y}_{mk}^p = \sqrt{\hat{p}_k}\tau_p \mathbf{A}\mathbf{K}_{1,m}\mathbf{h}_{mk} + \sum_{l\in\mathcal{P}_k\backslash\{k\}} \sqrt{\hat{p}_l}\tau_p \mathbf{A}\mathbf{K}_{1,m}\mathbf{h}_{ml} + \sum_{l\in\mathcal{P}_k} \sqrt{\hat{p}_l}\tau_p \mathbf{A}\mathbf{K}_{2,m}\mathbf{h}_{ml}^* + \mathbf{A}\mathbf{n}_{iqi,m}^p\phi_k^* + \check{\mathbf{n}}_{mq}^p\phi_k^*$.

The traditional MMSE estimators are widely adopted for estimating the channel with the prior information, e.g., the LoS component $\overline{\mathbf{h}}_{mk}$ and the spatial correlation matrix $\mathbf{R}_{mk}$. Based on the above and the phase-shift information φ_{mk}, the novel MMSE estimation criterion, that is so-called phase-aware MMSE estimator, is dedicated to the accuracy of channel estimation. So, if the channel statistics $\overline{\mathbf{h}}_{mk}, \mathbf{R}_{mk}$ are available and the phase-shift φ_{mk} is fully known at AP m, we can derive the phase-aware MMSE estimate of $\mathbf{h}_{mk}$ as Lemma 1.

Lemma 1: The Phase-Aware MMSE estimate of the channel from AP m to UE k is

$$\hat{\mathbf{h}}_{mk} = \overline{\mathbf{h}}_{mk}e^{j\varphi_{mk}} + \sqrt{\hat{p}_k}\mathbf{A}^H\mathbf{K}_{1,m}^H\mathbf{R}_{mk}\boldsymbol{\Psi}_{mk}^{-1}\left(\mathbf{y}_{mk}^p - \overline{\mathbf{y}}_{mk}^p\right), \quad (4)$$

where $\overline{\mathbf{y}}_{mk}^p = \sum_{l\in\mathcal{P}_k} \sqrt{\hat{p}_l}\tau_p \mathbf{A}\mathbf{K}_{1,m}\overline{\mathbf{h}}_{ml}e^{j\varphi_{ml}}$, and $\boldsymbol{\Psi}_{mk} = \sum_{l\in\mathcal{P}_k} \hat{p}_k\tau_p \mathbf{A}\mathbf{K}_{1,m}\mathbf{R}_{ml}\mathbf{K}_{1,m}^H\mathbf{A}^H + \sum_{l\in\mathcal{P}_k} \hat{p}_k\tau_p \mathbf{A}\mathbf{K}_{2,m}\mathbf{R}_{ml}^*\mathbf{K}_{2,m}^H\mathbf{A}^H + \mathbf{A}\boldsymbol{\Xi}\mathbf{A}^H + \mathbf{R}_{\check{\mathbf{n}}_{mq}^p}$.

The channel estimate $\hat{\mathbf{h}}_{mk}$ and estimation error $\tilde{\mathbf{h}}_{mk} = \mathbf{h}_{mk} - \hat{\mathbf{h}}_{mk}$ are independent random variables with $\mathbb{E}\{\hat{\mathbf{h}}_{mk}|\varphi_{mk}\} = \overline{\mathbf{h}}_{mk}e^{j\varphi_{mk}}$, $\mathrm{Cov}\{\hat{\mathbf{h}}_{mk}|\varphi_{mk}\} = \hat{p}_k\tau_p\boldsymbol{\Phi}_{mk}$, $\mathbb{E}\{\tilde{\mathbf{h}}_{mk}\} = \mathbf{0}$, $\mathrm{Cov}\{\tilde{\mathbf{h}}_{mk}\} = \mathbf{C}_{mk}$, and $\mathbf{C}_{mk} = \mathbf{R}_{mk} - \hat{p}_k\tau_p\boldsymbol{\Phi}_{mk}$, where $\boldsymbol{\Phi}_{mk} = \mathbf{A}\mathbf{K}_{1,m}\mathbf{R}_{mk}\boldsymbol{\Psi}_{mk}^{-1}\mathbf{R}_{mk}\mathbf{K}_{1,m}^H\mathbf{A}^H$.

C. Data Transmission

During the uplink data transmission, all the UEs send data signals to the APs simultaneously via the wireless propagation channels. The signal transmitted by UE k is s_k, with the power $p_k = \mathbb{E}\{|s_k|^2\}$. The received signal with the consideration of ADCs and IQI at AP m can be expressed as

$$\check{\mathbf{y}}_m = \sum_{k=1}^K \mathbf{A}\mathbf{K}_{1,m}\mathbf{h}_{mk}s_k + \sum_{k=1}^K \mathbf{A}\mathbf{K}_{2,m}\mathbf{h}_{mk}^*s_k^* + \mathbf{A}\mathbf{n}_{iqi,m} + \check{\mathbf{n}}_m, \quad (5)$$

where $\mathbf{n}_{iqi,m} = \mathbf{K}_{1,m}\mathbf{n}_m + \mathbf{K}_{2,m}\mathbf{n}_m^*$. And $\check{\mathbf{n}}_m$ is the Gaussian quantization noise, whose covariance matrix is given by (6) shown at the bottom of this page.

III. SPECTRAL EFFICIENCY ANALYSIS

In the uplink, we adopt the LSFD scheme, which can achieve better performance than fully-distributed implementation. We denote by $\mathbf{v}_{mk} \in \mathbb{C}^L$ the combining vector designed by AP m for UE k based on its local observation. In the first layer, the local estimate of s_k at AP m is given by

$$\tilde{s}_{mk} = \mathbf{v}_{mk}^H\check{\mathbf{y}}_m = \mathbf{v}_{mk}^H\mathbf{A}\mathbf{K}_{1,m}\mathbf{h}_{mk}s_k$$
$$+ \sum_{l=1,l\neq k}^K \mathbf{v}_{mk}^H\mathbf{A}\mathbf{K}_{1,m}\mathbf{h}_{ml}s_l$$
$$+ \sum_{l=1}^K \mathbf{v}_{mk}^H\mathbf{A}\mathbf{K}_{2,m}\mathbf{h}_{ml}^*s_l^* + \mathbf{v}_{mk}^H\mathbf{A}\mathbf{n}_{iqi,m} + \mathbf{v}_{mk}^H\check{\mathbf{n}}_m. \quad (7)$$

Note that $\mathbf{v}_{mk}$ varies from different linear combining methods. For MR combining, $\mathbf{v}_{mk} = \hat{\mathbf{h}}_{mk}$, and if we choose L-MMSE combining, then $\mathbf{v}_{mk}$ can be designed as

$$\mathbf{v}_{mk} = p_k \left(\begin{array}{c} \sum_{l=1}^K \mathbf{A}\mathbf{K}_{1,m}\hat{\mathbf{h}}_{ml}\hat{\mathbf{h}}_{ml}^H\mathbf{K}_{1,m}^H\mathbf{A}^H \\ + \sum_{l=1}^K \mathbf{A}\mathbf{K}_{2,m}\hat{\mathbf{h}}_{ml}^*\hat{\mathbf{h}}_{ml}^T\mathbf{K}_{2,m}^H\mathbf{A}^H \\ + \sum_{l=1}^K \tilde{\mathbf{C}}_{ml,1} + \sum_{l=1}^K \tilde{\mathbf{C}}_{ml,2} \\ + \mathbf{A}\boldsymbol{\Xi}\mathbf{A}^H + \mathbf{R}_{\check{\mathbf{n}}_m} \end{array} \right)^{-1} \hat{\mathbf{h}}_{mk}, \quad (8)$$

which can minimize the mean-squared error $\mathrm{MSE}_{mk} = \mathbb{E}\{|s_k - \mathbf{v}_{mk}^H\check{\mathbf{y}}_m|^2|\hat{\mathbf{h}}_{mk}\}$, where $\tilde{\mathbf{C}}_{ml,1} = \mathrm{diag}(\mathbf{A}\mathbf{K}_{1,m})\mathrm{diag}(\mathbf{K}_{1,m}^H\mathbf{A}^H) \odot \mathbf{C}_{ml}$, $\tilde{\mathbf{C}}_{ml,2} = \mathrm{diag}(\mathbf{A}\mathbf{K}_{2,m})\mathrm{diag}(\mathbf{K}_{2,m}^H\mathbf{A}^H) \odot \mathbf{C}_{ml}^*$.

The second layer of the decoding scheme is implemented in the CPU to mitigate the inter-user interference using LSFD coefficients. Compared with the small-scale coefficients, the large-scale coefficients vary slowly, relying on the distance between AP-UE pair and the environment. The local estimate $\tilde{s}_{mk}$ is sent to the CPU, where $\tilde{s}_{mk}$ is weighted by the LSFD coefficients. Therefore, we obtain the final decoding signal $\hat{s}_k = \sum_{m=1}^M a_{mk}^H\tilde{s}_{mk}$ as

$$\hat{s}_k = \sum_{m=1}^M \sum_{l=1}^K a_{mk}^H\mathbf{v}_{mk}^H\mathbf{A}\left(\mathbf{K}_{1,m}\mathbf{h}_{ml}s_l + \mathbf{K}_{2,m}\mathbf{h}_{ml}^*s_l^*\right)$$
$$+ \sum_{m=1}^M a_{mk}^H\mathbf{v}_{mk}^H\mathbf{A}\mathbf{n}_{iqi,m} + \sum_{m=1}^M a_{mk}^H\mathbf{v}_{mk}^H\check{\mathbf{n}}_m. \quad (9)$$

Then, we define the LSFD coefficient matrix $\mathbf{a}_k = [a_{1k}, \ldots, a_{Mk}]^T \in \mathbb{C}^M$, $\mathbf{g}_{kl,1} = [\mathbf{v}_{1k}^H\mathbf{A}\mathbf{K}_{1,1}\mathbf{h}_{1l}, \ldots, \mathbf{v}_{Mk}^H\mathbf{A}\mathbf{K}_{1,M}\mathbf{h}_{Ml}]^T \in \mathbb{C}^M$ and $\mathbf{g}_{kl,2} = [\mathbf{v}_{1k}^H\mathbf{A}\mathbf{K}_{2,1}\mathbf{h}_{1l}^*, \ldots, \mathbf{v}_{Mk}^H\mathbf{A}\mathbf{K}_{2,M}\mathbf{h}_{Ml}^*]^T \in \mathbb{C}^M$, respectively.

So, with the simplified representation above, (9) can be simplified as

$$\hat{s}_k = \mathbf{a}_k^H\mathbf{g}_{kk,1}s_k + \sum_{l=1,l\neq k}^K \mathbf{a}_k^H\mathbf{g}_{kl,1}s_l + \sum_{l=1}^K \mathbf{a}_k^H\mathbf{g}_{kl,2}s_l^*$$
$$+ \mathbf{n}_{k1} + \mathbf{n}_{k2}, \quad (10)$$

$$\mathbf{R}_{\check{\mathbf{n}}_{mq}^p} = \mathbf{A}\left(\mathbf{I}_L - \mathbf{A}\right)\mathrm{diag}\left(\mathbb{E}\left\{\mathbf{y}_{iqi,m}^p \left(\mathbf{y}_{iqi,m}^p\right)^H\right\}\right)$$
$$= \mathbf{A}\left(\mathbf{I}_L - \mathbf{A}\right)\mathrm{diag}\left(\sum_{k=1}^K \tau_p\hat{p}_k\mathbf{K}_{1,m}\mathbf{R}_{mk}\mathbf{K}_{1,m}^H + \sum_{k=1}^K \tau_p\hat{p}_k\mathbf{K}_{2,m}\mathbf{R}_{mk}^*\mathbf{K}_{2,m}^H + \boldsymbol{\Xi}\right). \quad (3)$$

$$\mathbf{R}_{\check{\mathbf{n}}_m} = \mathbf{A}\left(\mathbf{I}_L - \mathbf{A}\right)\mathrm{diag}\left(\sum_{k=1}^K p_k\mathbf{K}_{1,m}\mathbf{R}_{mk}\mathbf{K}_{1,m}^H + \sum_{k=1}^K p_k\mathbf{K}_{2,m}\mathbf{R}_{mk}^*\mathbf{K}_{2,m}^H + \boldsymbol{\Xi}\right). \quad (6)$$

where $\mathbf{n}_{k1} = \sum_{m=1}^{M} a_{mk}^H \mathbf{v}_{mk}^H \mathbf{A}\mathbf{n}_{iqi,m}$ and $\mathbf{n}_{k2} = \sum_{m=1}^{M} a_{mk}^H \mathbf{v}_{mk}^H \breve{\mathbf{n}}_m$.

Based on the received signal, we can derive the lower bound of uplink SE expressions using use-and-then-forget (UatF) bounding technique to analyze the system performance. So, the achievable SE of UE k is

$$\mathrm{SE}_k = \left(1 - \frac{\tau_p}{\tau_c}\right) \log_2 \left|1 + p_k \mathbf{F}_k^H \boldsymbol{\Sigma}_k^{-1} \mathbf{F}_k\right|, \qquad (11)$$

where $\mathbf{F}_k = \mathbf{a}_k^H \mathbb{E}\{\mathbf{g}_{kk,1}\}$ and $\boldsymbol{\Sigma}_k = p_k \sum_{l=1}^K \mathbf{a}_k^H \mathbb{E}\{\mathbf{g}_{kl,1}\mathbf{g}_{kl,1}^H\}\mathbf{a}_k + p_k \sum_{l=1}^K \mathbf{a}_k^H \mathbb{E}\{\mathbf{g}_{kl,2}\mathbf{g}_{kl,2}^H\}\mathbf{a}_k - \mathbf{F}_k\mathbf{F}_k^H + \mathbf{a}_k^H \mathbf{Z}_{k,1}\mathbf{a}_k + \mathbf{a}_k^H \mathbf{Z}_{k,2}\mathbf{a}_k$ with $\mathbf{Z}_{k,1} = \mathrm{tr}(\boldsymbol{\Xi}\mathbf{A}^H \mathbf{v}_k \mathbf{v}_k^H \mathbf{A}) = \mathrm{tr}(\boldsymbol{\Xi}\mathbf{v}_k\mathbf{v}_k^H \odot \mathrm{diag}(\mathbf{A})\mathrm{diag}(\mathbf{A}^H))$ and $\mathbf{Z}_{k,2} = \mathrm{tr}(\mathbf{R}_{\breve{\mathbf{n}}_m}\mathbb{E}\{\|\mathbf{v}_k\|^2\})$, respectively.

Actually, the LSFD coefficient matrix $\mathbf{a}_k$ can be optimized with the following corollary, then we can achieve the maximum of achievable SE.

Corollary 1: When the LSFD coefficient is chosen as

$$\mathbf{a}_k = p_k \begin{pmatrix} \sum_{l=1}^K \mathbb{E}\left\{\mathbf{g}_{kl,1}\mathbf{g}_{kl,1}^H\right\} \\ + \sum_{l=1}^K \mathbb{E}\left\{\mathbf{g}_{kl,2}\mathbf{g}_{kl,2}^H\right\} \\ + \mathbf{Z}_{k,1} + \mathbf{Z}_{k,2} \end{pmatrix}^{-1} \mathbb{E}\left\{\mathbf{g}_{kk,1}\right\}, \qquad (12)$$

we can get the maximum value of SE, shown as the equation (13) at the bottom of this page.

Furthermore, we focus on the closed-form SE expressions when the MR combining method is applied in the first layer rather than L-MMSE combining, which is shown as

$$\mathrm{SE}_k^c = \left(1 - \frac{\tau_p}{\tau_c}\right) \log_2 \left|1 + p_k \mathbf{F}_k^H \boldsymbol{\Sigma}_k^{-1} \mathbf{F}_k\right|, \qquad (14)$$

where $\mathbf{F}_k = \mathbf{a}_k^H \mathbf{Z}_k$, and $\mathbf{Z}_k = [\mathbf{Z}_{1k}, \ldots, \mathbf{Z}_{Mk}]^T$ with $\mathbf{Z}_{mk} = \mathbb{E}\{\mathbf{v}_{mk}^H \mathbf{A}\mathbf{K}_{1,m}\mathbf{h}_{mk}\} = \mathbb{E}\{\mathrm{tr}(\mathbf{A}\mathbf{K}_{1,m}\hat{\mathbf{h}}_{mk}\hat{\mathbf{h}}_{mk}^H)\} = \mathrm{tr}(\mathbf{A}\mathbf{K}_{1,m}\mathbb{E}\{\hat{\mathbf{h}}_{mk}\hat{\mathbf{h}}_{mk}^H\}) = \mathrm{tr}(\mathbf{A}\mathbf{K}_{1,m}(\boldsymbol{\Phi}_{mk} + \bar{\mathbf{h}}_{mk}\bar{\mathbf{h}}_{mk}^H))$. And we structure $\boldsymbol{\Theta}_{kl} = \mathbb{E}\{\mathbf{g}_{kl,1}\mathbf{g}_{kl,1}^H\} \in \mathbb{C}^{M\times M}$ into blocks, where the (m,n)-th element is $\boldsymbol{\Theta}_{kl}^{mn} = \mathbb{E}\{\mathbf{v}_{mk}^H \mathbf{A}\mathbf{K}_{1,m}\mathbf{h}_{ml}\mathbf{h}_{nl}^H \mathbf{K}_{1,n}^H \mathbf{A}^H \mathbf{v}_{nk}\} = \mathbb{E}\{\mathrm{tr}(\mathbf{A}\mathbf{K}_{1,m}\mathbf{h}_{ml}\mathbf{v}_{mk}^H)\mathrm{tr}(\mathbf{v}_{nk}\mathbf{h}_{nl}^H \mathbf{K}_{1,n}^H \mathbf{A}^H)\} = \mathrm{tr}(\mathbf{A}\mathbf{K}_{1,m}\mathbb{E}\{\mathbf{h}_{ml}\mathbf{v}_{mk}^H\})\mathrm{tr}(\mathbf{K}_{1,n}^H \mathbf{A}^H \mathbb{E}$

TABLE II
SIMULATION PARAMETERS

Symbol	Notion	Value
S	simulation area	1×1 km^2
δ_f	shadow fading parameter	0.5
d_{dc}	decorrelation distance	100 m
B	communication bandwidth	20 MHz
σ^2	noise power	-94 dBm
τ_c	length of coherence block	200
τ_p	pilot length	20
$\hat{p}_k$	transmit power of each UE	200 mW

$\{\mathbf{v}_{nk}\mathbf{h}_{nl}^H\}$), which is shown in (15) and (16) at the bottom of this page under two cases ($m = n$ and $m \neq n$), respectively. Since $\mathbb{E}\{\mathbf{h}_{mk}\mathbf{h}_{mk}^T\} = \mathbf{0}$, so we can get the closed-form result of $\boldsymbol{\Lambda}_{kl}^{mn} = \mathbb{E}\{\mathbf{g}_{kl,2}\mathbf{g}_{kl,2}^H\} \in \mathbb{C}^{M\times M} = \mathbf{0}$.

IV. NUMERICAL RESULTS

We investigate the impacts of the mixed-resolution ADCs and IQI on the CF mMIMO system for the simulation with a wrap-around scheme [9]. The simulation parameters are listed in Table II. All APs and UEs are uniformly distributed in S. We use the COST 321 Walfish-Ikegami model to describe the pathloss of CF mMIMO as $\mathrm{PL}_{m,k}[\mathrm{dB}] = -30.18 - 26\log_{10}(\frac{d_{mk}}{1\mathrm{m}}) + F_{m,k}$, where d_{mk} is the two-dimension distance of AP m-UE k pair, containing the horizontal distance and a vertical distance of 11 m. Furthermore, we let the Rician factor $\kappa_{m,k}$ equals to $10^{1.3-0.003d_{mk}}$.

$$\mathrm{SE}_{k,\max} = \left(1 - \frac{\tau_p}{\tau_c}\right)\log_2\left|1 + \mathbb{E}\left\{\mathbf{g}_{kk,1}^H\right\}\left(\begin{array}{c}\sum_{l=1}^K \mathbb{E}\left\{\mathbf{g}_{kl,1}\mathbf{g}_{kl,1}^H\right\} + \sum_{l=1}^K \mathbb{E}\left\{\mathbf{g}_{kl,2}\mathbf{g}_{kl,2}^H\right\} \\ + \mathbf{Z}_{k,1} + \mathbf{Z}_{k,2}\end{array}\right)^{-1}\mathbb{E}\left\{\mathbf{g}_{kk,1}\right\}\right|. \qquad (13)$$

$$\boldsymbol{\Theta}_{kl}^{mm} = \hat{p}_k\tau_p\mathrm{tr}\left(\mathbf{A}\mathbf{K}_{1,m}\mathbf{R}_{ml}\mathbf{K}_{1,m}^H \mathbf{A}^H \boldsymbol{\Phi}_{mk}\right) + \bar{\mathbf{h}}_{mk}^H \mathbf{A}\mathbf{K}_{1,m}\mathbf{R}_{ml}\mathbf{K}_{1,m}^H \mathbf{A}^H \bar{\mathbf{h}}_{mk} + \hat{p}_k\tau_p\bar{\mathbf{h}}_{ml}^H \mathbf{K}_{1,m}^H \mathbf{A}^H \boldsymbol{\Phi}_{mk}\mathbf{A}\mathbf{K}_{1,m}\bar{\mathbf{h}}_{ml} +$$

$$\left|\bar{\mathbf{h}}_{mk}^H \mathbf{A}\mathbf{K}_{1,m}\bar{\mathbf{h}}_{ml}\right|^2 + \begin{cases} 0, & l \notin \mathcal{P}_k \\ \hat{p}_k^2\tau_p^2\left|\mathrm{tr}\left(\left(\mathbf{A}^H\mathbf{K}_{1,m}^H\mathbf{R}_{mk}\boldsymbol{\Psi}_{mk}^{-1/2}\right)^H \mathbf{A}\mathbf{K}_{1,m}\left(\mathbf{A}^H\mathbf{K}_{1,m}^H\mathbf{R}_{mk}\boldsymbol{\Psi}_{mk}^{-1/2}\right)\right)\right|^2 \\ +2\hat{p}_k\tau_p\left\{\left(\mathbf{R}_{mk}\boldsymbol{\Psi}_{mk}^{-1/2}\right)^H \mathbf{A}\mathbf{K}_{1,m}\left(\mathbf{R}_{mk}\boldsymbol{\Psi}_{mk}^{-1/2}\right)\bar{\mathbf{h}}_{mk}\mathbf{K}_{1,m}^H \mathbf{A}^H \bar{\mathbf{h}}_{mk}\right\}, & l = k \\ \hat{p}_k\hat{p}_l\tau_p^2\left|\mathrm{tr}\left(\left(\mathbf{A}^H\mathbf{K}_{1,m}^H\mathbf{R}_{mk}\boldsymbol{\Psi}_{mk}^{-1/2}\right)^H \mathbf{A}\mathbf{K}_{1,m}\left(\mathbf{A}^H\mathbf{K}_{1,m}^H\mathbf{R}_{ml}\boldsymbol{\Psi}_{ml}^{-1/2}\right)\right)\right|^2, & l \in \mathcal{P}_k \setminus \{k\} \end{cases} \qquad (15)$$

$$\boldsymbol{\Theta}_{kl}^{mn} = \begin{cases} \mathrm{tr}\left(\mathbf{A}\mathbf{K}_{1,m}\bar{\mathbf{h}}_{ml}\bar{\mathbf{h}}_{mk}^H\right)\mathrm{tr}\left(\mathbf{K}_{1,n}^H \mathbf{A}^H \bar{\mathbf{h}}_{nk}\bar{\mathbf{h}}_{nl}^H\right), & l \notin \mathcal{P}_k \\ \mathrm{tr}\left(\mathbf{A}\mathbf{K}_{1,m}\left(\bar{\mathbf{h}}_{mk}\bar{\mathbf{h}}_{mk}^H + \boldsymbol{\Phi}_{mk}\right)\right)\mathrm{tr}\left(\mathbf{K}_{1,n}^H \mathbf{A}^H \left(\bar{\mathbf{h}}_{nk}\bar{\mathbf{h}}_{nk}^H + \boldsymbol{\Phi}_{nk}\right)\right), & l = k \\ \hat{p}_l\hat{p}_k\mathrm{tr}\left(\mathbf{A}\mathbf{K}_{1,m}\tau_p\mathbf{A}^H\mathbf{K}_{1,m}^H\mathbf{R}_{ml}\boldsymbol{\Psi}_{mk}^{-1}\mathbf{R}_{mk}^H\mathbf{K}_{1,m}\mathbf{A}\right)\mathrm{tr}\left(\mathbf{K}_{1,n}^H \mathbf{A}^H \tau_p\mathbf{A}^H\mathbf{K}_{1,n}^H\mathbf{R}_{nl}\boldsymbol{\Psi}_{nk}^{-1}\mathbf{R}_{nk}^H\mathbf{K}_{1,n}\mathbf{A}\right), & l \in \mathcal{P}_k \setminus \{k\} \end{cases} \qquad (16)$$
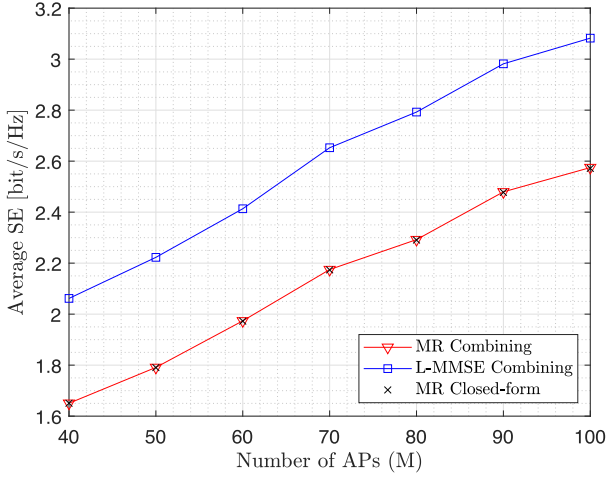
Fig. 1. Average SE versus the number of APs with L-MMSE combining and MR combining for $K = 40$, and $L = 4$.

Fig. 2. Average SE versus the antenna number of APs with MR/L-MMSE combining at different ADC architectures for $M = 80$, $K = 40$, and $L = 4$.

The shadow shading model is $F_{m,k} = \sqrt{\delta_f} a_m + \sqrt{1-\delta_f} b_k$, where $a_m \sim \mathcal{N}(0, \delta_{\mathrm{sf}}^2)$, $b_k \sim \mathcal{N}(0, \delta_{\mathrm{sf}}^2)$ are independent random variables, with the covariance functions of a_m and b_k are $\mathbb{E}\{a_m a_{m'}\} = 2^{\frac{-d_{m,m'}}{d_{\mathrm{dc}}}}$, $\mathbb{E}\{b_k b_{k'}\} = 2^{\frac{-d_{k,k'}}{d_{\mathrm{dc}}}}$, where $d_{m,m'}$ and $d_{k,k'}$ are the distances between AP m−AP m' pair and UE k−UE k' pair, respectively. Furthermore, the large-scale coefficients of the LoS path and NLoS path are given by $\beta_{mk}^{\mathrm{LoS}} = \sqrt{\frac{\kappa_{m,k}}{\kappa_{m,k}+1}} \sqrt{\mathrm{PL}_{m,k}}$, $\beta_{mk}^{\mathrm{NLoS}} = \frac{1}{\kappa_{m,k}+1} \mathrm{PL}_{m,k}$, respectively. Moreover, the n-th element of $\bar{\mathbf{h}}_{mk}$ is $[\bar{\mathbf{h}}_{mk}]_n = \sqrt{\beta_{mk}^{\mathrm{LoS}}} e^{j 2\pi d_H (n-1) \sin(\theta_{mk})}$ with d_H being the antenna spacing, where θ_{mk} is the angle of arrival to the UE k seen from AP m. Also, the (l, n)-th element of $\mathbf{R}_{mk}$ based on the Gaussian local scattering model is

$$[\mathbf{R}_{mk}]_n^l = \frac{\beta_{mk}^{\mathrm{NLoS}}}{\sqrt{2\pi}\sigma_\varphi} \int_{-\infty}^{+\infty} e^{j 2\pi d_H (l-n) \sin(\theta_{mk}+\delta)} e^{-\frac{\delta^2}{\sigma_\varphi^2}} d\delta, \quad (17)$$

where σ_φ is the angular standard deviation.

In Fig. 1, we investigate the average SE over Rician correlated fading channels with phase-shift as a function of the number of APs M for MR/L-MMSE combining. As the two lines shown in Fig. 1, the average SE increases with M. And there is a prominent promotion with the L-MMSE combining compared with MR combining, indicating that the L-MMSE combining can cope with the effect of IQI. Actually, this is because the L-MMSE combining can achieve the best balance between amplifying the desired signal and suppressing the interference. Furthermore, the accuracy of the derived uplink closed-form SE expressions for the MR combining has been verified since the "×" curve matches perfectly the results generated by the Monte-Carlo method.

In Fig. 2, we focus on the impact of the number of AP antennas and the resolution of ADCs on the average SE. Firstly, it is shown that the average SE increases with the AP antennas achieving more degrees of freedom, no matter whether with MR combining or L-MMSE combining. Furthermore, we can observe that the high-resolution ADCs can achieve the best SE performance and the SE performance of mixed-resolution ADCs architecture lies in between the high-resolution case and the low-resolution case. To be specific, the mixed-resolution ADCs with the MR combining can achieve nearly similar performance with the perfect, which indicates the merit of mixed-ADC architecture in CF mMIMO systems.
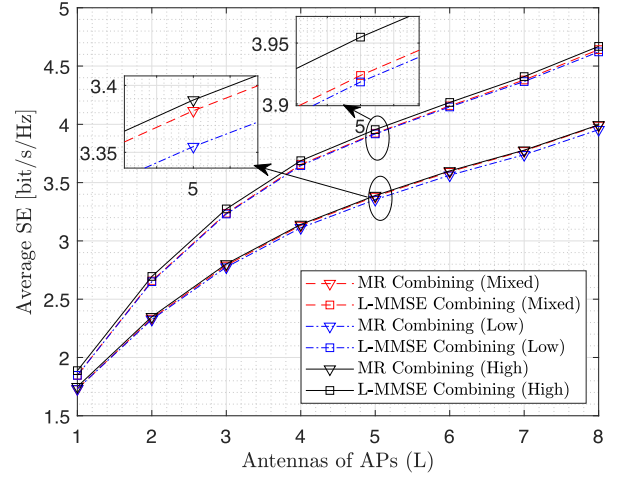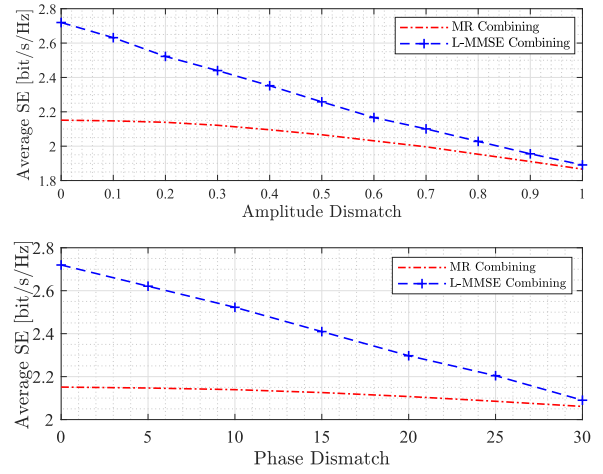

Fig. 3. Average SE versus the IQI parameters with L-MMSE combining and MR combining for $M = 60$, $K = 40$, and $L = 4$.

Fig. 3 shows the effect of different IQI coefficients with the MR/L-MMSE combining on the CF mMIMO system. The SE performance reaches its peak value of 2.72 b/s/Hz with the L-MMSE combining when there is no IQI. From both the sub-figures, we can observe that the L-MMSE combining is more sensitive to parameter changes, such as, when the maximum of amplitude mismatch is lower than 0.3, the average SE keeps steady with the MR combining while 10.28% decrement with the L-MMSE combining.

V. CONCLUSION

In this paper, we investigated the uplink SE performance for a CF mMIMO system with mixed-resolution ADCs and IQI over Rician spatially correlated channels. Based on a two-layer signal processing paradigm with the LSFD coefficients acquired, we derived the achievable SE expressions with MR combining and L-MMSE combining. Furthermore, we also computed the closed-form SE expression for the CF mMIMO system with MR combining. Moreover, in numerical results, we investigated the impacts of mixed-resolution ADCs and IQI on the CF mMIMO system. The numerical results showed that L-MMSE combining can significantly enhance the SE performance compared with MR combining influenced by the quantization distortion

and IQI. Furthermore, the ADCs with mixed-resolution can achieve a tradeoff between the one-bit ADCs and perfect ADCs. However, the effect of IQI, especially the amplitude mismatch, is harmful to the average SE performance. In future work, we will investigate the hardware effects and propose effective IQI compensation strategies to bridge the gap caused by hardware.

REFERENCES

[1] J. Zhang, E. Björnson, M. Matthaiou, D. W. K. Ng, H. Yang, and D. J. Love, "Prospective multiple antenna technologies for beyond 5G," *IEEE J. Sel. Areas Commun.*, vol. 38, no. 8, pp. 1637–1660, Aug. 2020.

[2] H. Du et al., "Semantic communications for wireless sensing: RIS-aided encoding and self-supervised decoding," Nov. 2022, *arXiv:2211.12727*.

[3] E. Shi et al., "Wireless energy transfer in RIS-aided cell-free massive MIMO systems: Opportunities and challenges," *IEEE Commun. Mag.*, vol. 60, no. 3, pp. 26–32, Mar. 2022.

[4] H. Du et al., "Performance and optimization of reconfigurable intelligent surface aided THz communications," *IEEE Trans. Commun.*, vol. 70, no. 5, pp. 3575–3593, May 2022.

[5] Q. Ding and Y. Jing, "SE analysis for mixed-ADC massive MIMO uplink with ZF receiver and imperfect CSI," *IEEE Wireless Commun. Lett.*, vol. 9, no. 4, pp. 438–442, Apr. 2020.

[6] S. Chen, J. Zhang, E. Björnson, J. Zhang, and B. Ai, "Structured massive access for scalable cell-free massive MIMO systems," *IEEE J. Sel. Areas Commun.*, vol. 39, no. 4, pp. 1086–1100, Apr. 2021.

[7] Z. Wang, J. Zhang, B. Ai, C. Yuen, and M. Debbah, "Uplink performance of cell-free massive MIMO with multi-antenna users over jointly-correlated rayleigh fading channels," *IEEE Trans. Wireless Commun.*, vol. 21, no. 9, pp. 7391–7406, Sep. 2022.

[8] H. Q. Ngo, A. Ashikhmin, H. Yang, E. G. Larsson, and T. L. Marzetta, "Cell-free massive MIMO versus small cells," *IEEE Trans. Wireless Commun.*, vol. 16, no. 3, pp. 1834–1850, Mar. 2017.

[9] E. Björnson and L. Sanguinetti, "Making cell-free massive MIMO competitive with MMSE processing and centralized implementation," *IEEE Trans. Wireless Commun.*, vol. 19, no. 1, pp. 77–90, Jan. 2020.

[10] T. C. Mai, H. Q. Ngo, and L.-N. Tran, "Energy efficiency maximization in large-scale cell-free massive MIMO: A projected gradient approach," *IEEE Trans. Wireless Commun.*, vol. 21, no. 8, pp. 6357–6371, Aug. 2022.

[11] Z. Liu, J. Zhang, Z. Wang, and H. Q. Ngo, "Cell-free massive MIMO with low-resolution ADCs and I/Q imbalance over spatially correlated channels," in *Proc. IEEE Glob. Commun. Conf.*, 2022, pp. 2450–2455.

[12] Y. Zhang, Y. Cheng, M. Zhou, L. Yang, and H. Zhu, "Analysis of uplink cell-free massive MIMO system with mixed-ADC/DAC receiver," *IEEE Syst. J.*, vol. 15, no. 4, pp. 5162–5173, Dec. 2021.

[13] S. Shekhar, A. Subhash, M. Srinivasan, and S. Kalyani, "Joint power-control and antenna selection in user-centric cell-free systems with mixed resolution ADC," *IEEE Trans. Commun.*, vol. 70, no. 12, pp. 8400–8415, Dec. 2022.

[14] A. Papazafeiropoulos, E. Björnson, P. Kourtessis, S. Chatzinotas, and J. M. Senior, "Scalable cell-free massive MIMO systems: Impact of hardware impairments," *IEEE Trans. Veh. Technol.*, vol. 70, no. 10, pp. 9701–9715, Oct. 2021.

[15] I.-S. Kim, M. Bennis, and J. Choi, "Cell-free mmWave massive MIMO systems with low-capacity fronthaul links and low-resolution ADC/DACs," *IEEE Trans. Veh. Technol.*, vol. 71, no. 10, pp. 10512–10526, Oct. 2022.

[16] J. Zheng, J. Zhang, L. Zhang, X. Zhang, and B. Ai, "Efficient receiver design for uplink cell-free massive MIMO with hardware impairments," *IEEE Trans. Veh. Technol.*, vol. 69, no. 4, pp. 4537–4541, Apr. 2020.

[17] Y. Xiong, S. Sun, L. Qin, N. Wei, L. Liu, and Z. Zhang, "Performance analysis on cell-free massive MIMO with capacity-constrained fronthauls and variable-resolution ADCs," *IEEE Syst. J.*, vol. 16, no. 2, pp. 3296–3307, Jun. 2022.

[18] X. Wang, Y. Gao, N. Sha, M. Guo, and N. Li, "Secrecy performance analysis of mixed-ADC/DAC cell-free massive MIMO in the presence of multiple eavesdroppers," *IEEE Trans. Green Commun. Netw.*, vol. 7, no. 2, pp. 759–771, Jun. 2023.

[19] Z. Wang, J. Zhang, E. Björnson, and B. Ai, "Uplink performance of cell-free massive MIMO over spatially correlated Rician fading channels," *IEEE Commun. Lett.*, vol. 25, no. 4, pp. 1348–1352, Apr. 2021.

[20] J. Zheng, J. Zhang, E. Björnson, Z. Li, and B. Ai, "Cell-free massive MIMO-OFDM for high-speed train communications," *IEEE J. Sel. Areas Commun.*, vol. 40, no. 10, pp. 2823–2839, Oct. 2022.